X-ray absorption near edge structure/electron energy loss near edge structure calculation using the supercell orthogonalized linear combination of atomic orbitals method

2009 J. Phys.: Condens. Matter 21 104202

(http://iopscience.iop.org/0953-8984/21/10/104202)

IOP PUBLISHING JOURNAL OF PHYSICS: CONDENSED MATTER

J. Phys.: Condens. Matter **21** (2009) 104202 (16pp) doi:10.1088/0953-8984/21/10/104202

X-ray absorption near edge structure/electron energy loss near edge structure calculation using the supercell orthogonalized linear combination of atomic orbitals method

Wai-Yim Ching and Paul Rulis

Department of Physics, University of Missouri-Kansas City, Kansas City, MO 64110, USA

Received 27 September 2008
Published 10 February 2009
Online at stacks.iop.org/JPhysCM/21/104202

Abstract

Over the last eight years, a large number of x-ray absorption near edge structure (XANES) and/or electron energy loss near edge structure (ELNES) spectroscopic calculations for complex oxides and nitrides have been performed using the supercell-OLCAO (orthogonalized linear combination of atomic orbitals) method, obtaining results in very good agreement with experiments. The method takes into account the core-hole effect and includes the dipole matrix elements calculated from *ab initio* wavefunctions. In this paper, we describe the method in considerable detail, emphasizing the special advantages of this method for large complex systems. Selected results are reviewed and several hitherto unpublished results are also presented. These include the Y K edge of Y ions segregated to the core of a $\Sigma 31$ grain boundary in alumina, O K edges of water molecules, C K edges in different types of single walled carbon nanotubes, and the Co K edge in the cyanocobalamin (vitamin B_{12}) molecule. On the basis of these results, it is argued that the interpretation of specific features of the calculated XANES/ELNES edges is not simple for complex material systems because of the delocalized nature of the conduction band states. The long-standing notion of the 'fingerprinting' technique for spectral interpretation of experimental data is not tenable. A better approach is to fully characterize the structure under study, using either crystalline data or accurate *ab initio* modeling. Comparison between calculated XANES/ELNES spectra and available measurements enables us to ascertain the validity of the modeled structure. For complex crystals or structures, it is necessary to use the weighted sum of the spectra from structurally nonequivalent sites for comparison with the measured data. Future application of the supercell-OLCAO method to complex biomolecular systems is also discussed.

(Some figures in this article are in colour only in the electronic version)

1. Introduction

Within the last two decades or so there have been tremendous developments in the experimental probes of the unoccupied states in solids using x-ray absorption near edge structure (XANES) [1–3] and electron energy loss near edge structure (ELNES) spectroscopy [4, 5]. This is mainly due, on one hand, to the availability of high intensity x-ray sources offered by the establishment of many synchrotron radiation centers (SRC) worldwide. On the other hand, the advancement of high resolution transmission electron microscopy (HRTEM) and, more recently, scanning transmission electron microscopy (STEM) in conjunction with electron energy loss spectroscopy (EELS) as an effective materials characterization tool has also yielded unprecedented amounts of data on many types of different material systems [6–10]. To properly interpret the measured spectral data and to understand the underlying physics, theoretical calculations have become indispensable.

This has resulted in the development of many computational methods which were further assisted by timely advances in the electronic structure theory of solids within the same period, especially the local density approximation (LDA) of density functional theory (DFT). Together with the wide availability of ever faster computers, more realistic calculations could be extended to systems of greater complexity and with increased accuracy.

There are now several well established methods for XANES/ELNES calculation. These methods either use different computational approaches, or cover different energy ranges of interest, or focus on different aspects of the underlying theory with attendant approximations [11–15]. These methods and approaches have been amply described by other leading researchers who contributed to this special issue as summarized by Tanaka [16]. Among these methods, the orthogonalized linear combination of atomic orbitals (OLCAO) method in the supercell implementation has demonstrated itself to be an efficient and accurate method for XANES/ELNES spectral calculations and is especially suitable for large complex systems. Ostensibly, the supercell-OLCAO method has not been widely recognized since it has been used by only a few groups within the last few years. The motivation of this review article is therefore to give a detailed account of the supercell-OLCAO method; to point out its special advantages and also some of the current limitations, and to outline the directions that it can be further improved to meet greater challenges ahead. In spite of the limited publicity, a large number of calculations on many crystals and defective structures of increasing complexity have been performed using the supercell-OLCAO method. They are succinctly reviewed in this article. Based on these extensive calculations, we point out the failure of the prevailing concept of 'fingerprinting', which is routinely used to interpret XANES/ELNES spectra, beyond a set of very limited special cases. Additional results obtained by the supercell-OLCAO method, including some new unpublished results, are presented to illustrate these points.

2. Review of the supercell-OLCAO method

We start with a brief description of the OLCAO method in the context of electronic structure theory. The OLCAO method has its roots in the traditional LCAO method which itself has a long history starting in the early days of the quantum theory of solids [17]. The OLCAO method [18], being an all-electron method, contains the core orbitals in the basis expansion but the core orbitals are later eliminated by the orthogonalization procedure from the final secular equation [19], thereby reducing its dimension. This is in the same spirit as the orthogonalized plane wave method (OPW) [20]. However, it should be pointed out that the purpose of the OPW method was to speed up the convergence in the number of plane waves needed for the basis expansion. It never became practical and was later replaced by much more practical and robust methods such as the plane wave pseudopotential method, the augmented plane wave method (APW), and its linearized version (LAPW) as implemented in many popular codes such as CASTEP, VASP, Abinit, Wien2k, etc. The purpose of orthogonalization in the OLCAO method is mainly to reduce the dimension of the secular equation so that it can be applied to much larger systems (measured in terms of the number of electrons in the system). There are other methods in both quantum chemistry and in condensed matter theory similar to LCAO or OLCAO methods but they differ in the type of basis used or in their implementation. These methods will not be reviewed in this article.

2.1. Fundamentals of the OLCAO method

In the OLCAO method for periodic solids, the solid state wavefunction $\Psi_{nk}(\vec{r})$ is expanded in terms of Bloch sums $b_{i\alpha}(\vec{k},\vec{r})$.

$$\Psi_{nk}(\vec{r}) = \sum_{i,\alpha} C^n_{i\alpha}(\vec{k}) b_{i\alpha}(\vec{k},\vec{r}) \tag{1}$$

$$b_{i\alpha}(\vec{k},\vec{r}) = \left(\frac{1}{\sqrt{N}}\right) \sum_{\upsilon} e^{i\vec{k}\cdot\vec{R}_\upsilon} u_i(\vec{r} - \vec{R}_\upsilon - \vec{t}_\alpha). \tag{2}$$

Here, n is the band index, $\vec{k}$ is the wavevector, $C^n_{i\alpha}$ is the wavefunction (eigenvectors), (i,α) is a pair of indices specifying the orbital and atomic state, and υ is the index for the lattice. The $u_i(\vec{r} - \vec{r}_{\vec{A}})$ are the atomic orbitals i centered at the atomic site $\vec{A}$ whose radial part is expanded in terms of N Gaussian type orbitals (GTOs) and whose angular part is the usual set of spherical harmonics $Y_{lm}(\theta,\phi)$.

$$u_i(\vec{r}) = [\Sigma_j^N A_j r^{n-1} \mathrm{e}^{-\alpha_j r^2}] \cdot Y_{l,m}(\theta,\varphi). \tag{3}$$

In (3), the atomic orbital i collectively represent the principle quantum number n (not to be confused with the band index n in (1)) and the angular quantum numbers (l,m). The GTO in (3) is characterized by a decaying exponential α_j (not to be confused with the label α for the atomic sites in (2)). $\{\alpha_j\}$ and the expansion coefficients $\{A_j\}$ are carefully constructed and tested for each atomic type and stored in the OLCAO data base.

In the OLCAO method, three types of atomic basis expansions are used: minimal basis (MB), full basis (FB), and extended basis (EB). The MB consists of the core orbitals and orbitals in the valence shell of the atom. It is used mostly for calculations of effective charges and bond order values based on Mullikan population analysis [21] where the basis function used should be more localized. The FB includes an extra shell of orbitals beyond the MB. For most electronic structure calculations the FB is more than sufficient. In cases where highly excited states are desired, such as in the XANES/ELNES calculations, the EB is used which includes additional higher atomic orbitals than the FB. There is no fixed rule for designating the boundaries between a MB, FB, or EB in the OLCAO data base. Much of these are based on past experience and the nature of the problem to be solved. As an example, for the element Si, the MB consists of the core orbitals (1s, 2s, 2p) and the valence orbitals (3s, 3p). The FB has 3d, 4s, and 4p added to it, and the EB have additional excited state orbitals of 4d, 5s, and 5p. Depending on the type of the problem to be solved, sometimes the 3d orbital is

included in the MB for Si to address the possible s–d and p–d interactions. Likewise certain semi-core orbitals (such as Ca 3p or Ge 3d) are considered to be in the valence shell. It is such flexibility in the basis expansion that makes the OLCAO method extremely versatile with virtually no limitations on the type of crystals it can be applied to. Over the years, the OLCAO method has been successfully used to study the electronic structure and optical properties of many different types of crystals.

As in any electronic structure method, the central step is to solve the Kohn–Sham equation at various k-points in the Brillouin zone (BZ), or equivalently diagonalize the secular equation:

$$|H_{i\alpha,j\beta}(\vec{k}) - E(\vec{k})S_{i\alpha,j\beta}(\vec{k})| = 0 \tag{4}$$

where $S_{i\alpha,j\beta}(\vec{k})$ and $H_{i\alpha,j\beta}(\vec{k})$ are the overlap and Hamiltonian matrices.

$$\begin{aligned} S_{i\alpha,j\beta}(\vec{k}) &= \langle b_{i\alpha}(\vec{k},\vec{r}) \mid b_{j\beta}(\vec{k},\vec{r})\rangle \\ &= \sum_v e^{i\vec{k}\cdot\vec{R}_v} \int u_i(\vec{r}-\vec{t}_\alpha)u_j(\vec{r}-\vec{R}_v-\vec{t}_\beta)\,d\vec{r} \end{aligned} \tag{5}$$

$$\begin{aligned} H_{i\alpha,j\beta}(\vec{k}) &= \langle b_{i\alpha}(\vec{k},\vec{r})|H|b_{j\beta}(\vec{k},\vec{r})\rangle \\ &= \sum_v e^{i\vec{k}\cdot\vec{R}_v} \int u_i(\vec{r}-\vec{t}_\alpha)[-\nabla^2 + V_{\mathrm{Coul}}(\vec{r}) + V_{\mathrm{ex}}(\vec{r})] \\ &\quad \times u_j(\vec{r}-\vec{R}_v-\vec{t}_\beta)\,d\vec{r}. \end{aligned} \tag{6}$$

In the above, the overlap matrix involves summation over two-center integrals with atomic orbitals at two different sites. The Hamiltonian matrix consists of the kinetic energy term, the Coulomb potential term and the exchange–correlation term. The kinetic energy part is a two-center integral and the potential parts are three-center integrals since the crystal potential $V(\vec{r})$ is cast as the superposition of atom-centered functions $V_{\mathrm{A}}(\vec{r})$. Each of these atom-centered potential functions combines the Coulomb and exchange–correlation parts, and is collectively expressed as a sum of Gaussian orbitals.

$$\begin{aligned} V_{\mathrm{cry}}(\vec{r}) &= \Sigma_\alpha V_{\mathrm{A}}(\vec{r}-\vec{t}_\alpha) \\ &= -\frac{Z_{\mathrm{A}}}{r}\exp(-\eta r^2) + \Sigma_{j=1}^{N} D_j \exp(-\beta_j r^2). \end{aligned} \tag{7}$$

In (7), Z_{A} is the atomic number, η is a fixed damping parameter ($\sim$20). The charge density $\rho(\vec{r})$ of the crystal, which is required in the evaluation of the potential at each iteration in the SCF solution of the Kohn–Sham equation, is also expressed as a sum of Gaussians where the set of Gaussian exponentials $\{\beta_j\}$ are chosen to be the same set as in the potential representation.

$$\rho_{\mathrm{cry}}(\vec{r}) = \Sigma_\alpha \rho_{\mathrm{A}}(\vec{r}-\vec{t}_\alpha) = \Sigma_{j=1}^{N} B_j \exp(-\beta_j r^2). \tag{8}$$

The set $\{\beta_j\}$ is again chosen carefully for each type of atom and the corresponding expansion coefficients $\{D_j\}$ and $\{B_j\}$ are initially chosen from single atom calculations, but they are iteratively updated in the self-consistent cycles until convergence in the potential is attained.

All the multi-center integrals can be expressed in analytic forms via the technique of Gaussian transformation [22]. The efficiency of the OLCAO method is rooted in the analytic expression for the interaction integrals in direct space and the judicious choice of the Gaussian exponentials representing the one-electron LDA potential and charge density as well as the radial part of the basis function. The computational burden is further reduced by the orthogonalization scheme [19] in which the core orbitals are eliminated from the final secular equation, making it particularly suitable for large systems with large numbers of electrons.

2.2. Supercell-OLCAO method for XANES/ELNES calculations

The OLCAO method was later extended to the supercell-OLCAO method and specifically designed for XANES/ELNES calculations [23]. In this method, the core orbitals of the target atom whose absorption edges are to be calculated are retained while the core orbitals of all other atoms in the supercell are eliminated by orthogonalization. For a supercell of sufficiently large size, the corresponding BZ is very small. We can use just one $\vec{k}$ point either at the BZ center or at a general $\vec{k}$ point within the BZ. The index $\vec{k}$ can then be dropped.

The general theory for the XANES/ELNES calculation in solids is based on quantum scattering theory and has been extensively reviewed in many articles [5, 24–30]. Experimentally, the measured quantity is the inelastic partial differential scattering cross section of the incoming particle (a photon or an electron):

$$\frac{d^2\sigma}{d\Omega\,dE} = \frac{1}{(\pi e a_0)q^2}\mathrm{IM}\left\{\frac{-1}{\varepsilon(\vec{q},\hbar\omega)}\right\}. \tag{9}$$

where $\varepsilon(\vec{q},\hbar\omega)$ is the microscopic complex dielectric function and IM stands for the imaginary part. For small momentum transfer and at energies far above the plasma frequency $IM\{-1/\varepsilon(\vec{q},\hbar\omega)\}$, can be approximated as $\varepsilon_2(0,\hbar\omega)$ with no $\vec{q}$ dependence. The transition probability I per unit time for the inner shell core excitation within the dipole approximation can be reduced to the following simple expression according to the Fermi golden rule [31].

$$I \propto \sum_n |\langle g|\vec{r}|f\rangle|^2 \delta(E_f - E_g - \hbar\omega) \tag{10}$$

where g and f stand for the initial ground state and the final state with respective energies of E_g and E_f. The summation in (10) is over all final states. In the context of one-electron band theory, the initial state g is the atomic-like core state of the target atom in the solid and f are the final states which span all conduction band (CB) states.

In the early days of XANES/ELNES calculation, the matrix elements in (10) were approximated by the orbital resolved partial density of states (PDOS) of the CB with specific angular momentum symmetry. This is based on the fact that the atomic core level in the ground state is highly localized and orthogonal to the final states. The dipole selection rule restricts the transition from the 1s core state ($\ell = 0$) to only the p states ($\ell = 1$) in the CB and the transition from the 2p core state ($\ell = 1$) can only be to s or d type states ($\ell = 0$ or 2). However, in many instances, this approximation is found to be a poor one because the CB states are generally

delocalized and there is no precise way of decomposing them into different components of specific angular momentum. In the supercell-OLCAO method, the dipole matrix elements of transition between the initial and final states are explicitly included, and the selection rules are automatically imposed by the symmetry of the wavefunctions.

In XANES/ELNES calculations for insulators, it was recognized early on that the core-hole effect [32–34] is very important and must be properly accounted for. When an electron is excited from the inner core shell to the CB of the solid, it leaves behind a positively charged hole in the core (core-hole) which interacts with the excited electron in the CB, a process analogous to the excitonic effect in semiconductors. In metals, the effective screening by the CB electrons reduces the interaction and the core-hole effect is less important [35, 36]. There are two approaches to account for the core-hole effect. The first one is the $Z + 1$ approach based on the assumption that the presence of a core hole can be mimicked by replacing the atomic number (Z) of the target atom with that of another atom of a higher atomic number $(Z + 1)$ [37, 38]. The second one is to use the Slater transition scheme where a half-electron is removed from the core orbital and put at the lowest unoccupied state [39, 40]. A single diagonalization of the secular equation gives the transition energy ΔE. The final spectrum is obtained by combining ΔE and the oscillator strength from the dipole matrix elements calculated between the initial and final states. Both approaches have their drawbacks. For example, the $Z + 1$ approach cannot distinguish the effect of the core-hole for transitions from different core levels. The Slater transition scheme does not accurately reflect the actual interaction between the core hole and the excited electron.

In the supercell-OLCAO method, a different approach is used to account for the core-hole effect. The initial state and the final states are calculated separately at the level of LDA theory [41, 42]. The initial state is the ground state of the supercell with the core states of the targeted atom retained in the orthogonalization procedure. The final states are obtained by placing a core electron in the lowest CB state and the resulting Kohn–Sham equation is solved self consistently. It is assumed that the self-consistent solution of the final states accounts for all the multiple scattering effects of the excited electron in the CB and its interaction with the core-hole. The electron–core-hole interaction greatly modifies the final state wavefunction, and is the single most important factor for accurate reproduction of the measured spectra [23]. The placement of the excited electron from the core to the CB is important since it maintains the charge neutrality condition necessary for all electronic structure calculations. The core-hole effect cannot be accurately accounted for without using a supercell. This is because the theory is based on a single electron process where only one core-hole in the target atom is present while the band theory of solids is based on the Bloch Theorem of the periodic lattice. If a primitive cell or a small supercell is used, there will be spurious interactions between the core-hole and those of the image atoms in the adjacent periodic cell. This is illustrated schematically in figure 1. The size of the supercell used must be sufficiently large and

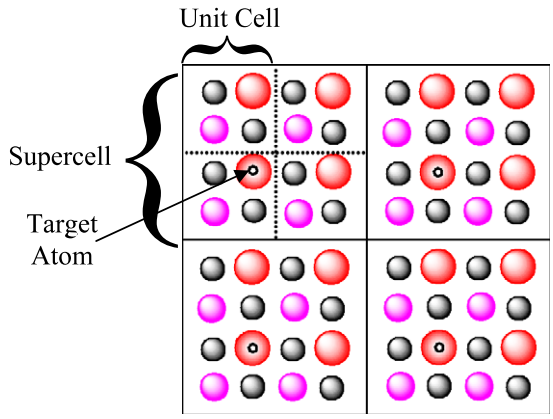

Figure 1. Supercell scheme for XANES/ELNES calculations.

carefully chosen for accuracy. A small supercell results in considerable interaction between the adjacent core-holes. Too large a supercell increases the computational burden. The size of the supercell is determined mainly by the shortest distance of separation from the core-holes in the adjacent cell. Thus a cubic cell usually has a much smaller number of atoms in the supercell than an anisotropic elongated crystalline cell for the same distance of separation. Past experience indicates that a distance of separation of about 9 Å should be sufficient depending on the system to be studied. For a cubic system, this amounts to about 100 atoms at most. For highly anisotropic crystals, or for models involving microstructures or interfaces, the calculations could involve supercells containing up to several hundred atoms. So, the calculation treats highly anisotropic crystals and those with light elements (shorter bond lengths) less favorably.

The final calculation of the XANES/ELNES spectrum in the supercell-OLCAO method entails the evaluation of equation (10) for the transition intensity between the initial core state and final core-hole states which are calculated separately. It can be easily shown that the dipole matrix in equation (10) is equivalent to the momentum matrix element in the optical transition calculation in the usual OLCAO method represented by the imaginary part of the frequency-dependent dielectric function $\varepsilon_2(\hbar\omega)$ [18]:

$$\langle g|\vec{r}|f\rangle \rightarrow M_{i\alpha,j\beta} = \langle b_{i\alpha}|\vec{\nabla}|b_{j\beta}\rangle = \sum_{\upsilon}\int u_i(\vec{r}-\vec{t}_\alpha)\vec{\nabla}u_j(\vec{r}-\vec{R}_\upsilon-\vec{t}_\beta)\,\mathrm{d}\vec{r}. \tag{11}$$

$$\varepsilon_2(\hbar\omega) = \left(\frac{e^2}{\pi m\omega^2}\right)\times\int \mathrm{d}\vec{k}\sum_{n,l}|\langle\psi_n(\vec{k},\vec{r})|\vec{P}\times|\psi_l(\vec{k},\vec{r})\rangle|^2\delta(E_f-E_g-\hbar\omega). \tag{12}$$

The momentum matrix elements in (12) are two-center integrals and can be efficiently evaluated analytically. The square of the momentum matrix in (12) can be resolved into Cartesian directions enabling the study of anisotropy in the calculation of the XANES/ELNES spectra. The explicit inclusion of the dipole transition matrix in the calculation of the XANES/ELNES spectrum is important since it provides more accurate amplitudes of transition in the spectral features. In

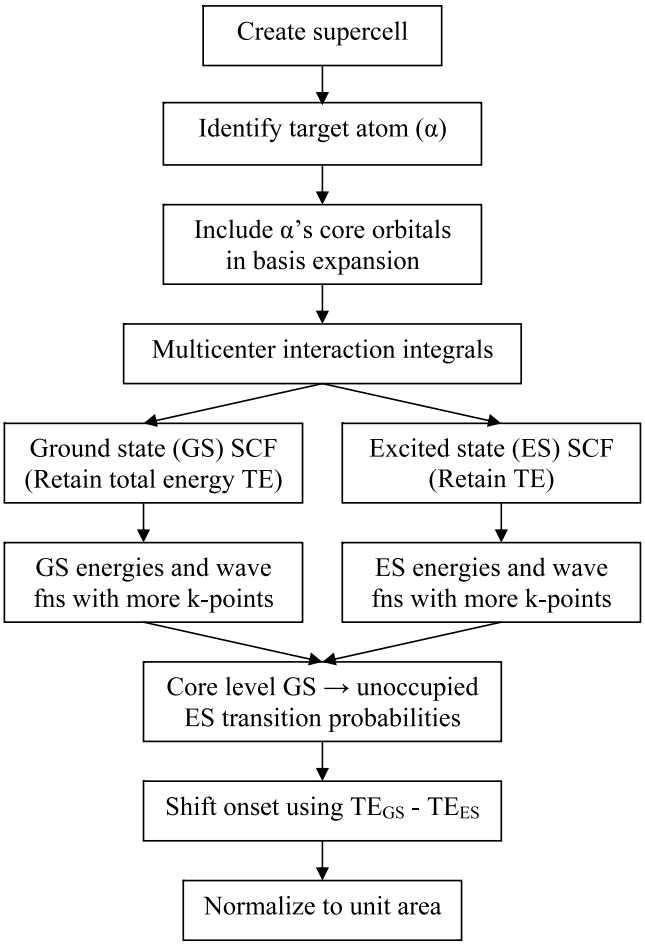

Figure 2. Flowchart for XANES/ELNES calculation using the supercell-OLCAO method.

the current implementation of the supercell-OLCAO method, a Gaussian broadening with a FWHM of 1.0 eV is applied to all calculated spectra to account for the life-time broadening. In other words, no attempt is made to use the broadening procedure itself as a means to achieve a better agreement with experiment. There are research efforts specifically dedicated to this issue of life-time broadening in order to better understand the actual process in the experiments and improve agreement with measured data. The broadening of the spectrum can depend on the excitation energy and also the instrumentation. This is a subject for future development and improvement in the supercell-OLCAO XANES/ELNES calculation. In the present implementation of the supercell-OLCAO method, all spectra for the same edge from the same atomic type are normalized to the same area. The specific procedures of the XANES/ELNES calculation using the supercell-OLCAO method are summarized in the flow chart shown in figure 2.

2.3. Special advantages of the supercell-OLCAO method

Before we review the vast amount of XANES/ELNES calculations using the supercell-OLCAO method, it is imperative to point out some special advantages of the method that make such calculations possible. Like any other method, there are ways that the method can still be improved while it also faces certain inherent limitations. These will be discussed in a later section. Still, we believe that the supercell-OLCAO method is among the most competitive methods for XANES/ELNES calculations, especially for systems with large and complex structures. These advantages are listed below.

First, the fundamental theory in the OLCAO method for electronic structure calculation is solid within the framework of the DFT. Although many-body interactions are not considered in the method, the separate calculation for the ground state and the final states is one step beyond the usual one-electron approximation since the electron–hole interaction is accounted for via the self-consistent iterations of the Kohn–Sham equation for the final states.

Second, the OLCAO method is an all-electron method with the core states explicitly included in the basis expansion. The physical presence of the core hole in the method and its explicit interaction with the electron in the CB distinguishes itself from other approaches where the core is described by an effective potential. The full secular equation is diagonalized to obtain all-electron states. When an EB is used, the CB states at a very high energy can be obtained to get the XANES/ELNES spectra up to 40–50 eV from the absorption edge on-set. In contrast, if an iterative procedure is used, only a small number of CB state wave functions are usually obtained. To obtain CB states at a high energy range could be computationally prohibitive. Of course, the full diagonalization of a large secular equation for large complex systems can also be a computational burden. On balance, the supercell-OLCAO method is still advantageous, as can be seen by its robust application to many complex systems.

Third, the dipole matrix elements of transition between the initial ground state and the final core-hole states are accurately calculated from the *ab initio* wave functions and explicitly included in the spectral calculation. These dipole matrix elements automatically impose the selection rules for the transition and the PDOS of the CB states play no role in the calculation. Of course it is still possible to use the PDOS which can be easily obtained in the OLCAO method for the interpretation of the final spectrum. The dipole matrix elements can also be resolved into Cartesian components to investigate the anisotropy of the XANES/ELNES spectra.

Fourth, the transition energy ΔE for each absorption edge can be obtained from the difference in the total energies of the ground state (N electrons in the core level and the VB) and the final state ($N-1$ electrons with an extra electron in the CB). Although the theoretical ΔE can never reproduce the experimental transition energy at the edge on-set and may depend on the size of the supercell, it is usually within a few per cent of the experimental transition energy. It is very useful for comparing different spectra of the same edge at different sites or in different crystals, as long as the same computational procedure is used in the calculation. The ability to relate ΔE to experimental spectra is very important. This is because the measured spectrum of a particular atom in a crystal is usually the weighted sum of the spectra from atoms at nonequivalent sites with slightly different local environments.

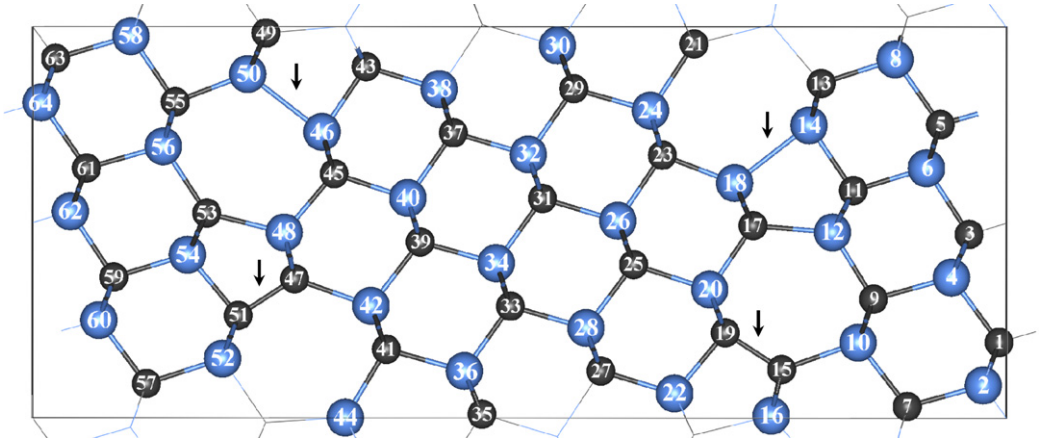

Figure 3. SiC–GB non-polar model. Large (small) spheres represent Si (C). The arrows indicate the wrong Si–Si and C–C bonds.

A slight difference in ΔE will result in a substantially different total spectrum when combined. This will be illustrated by specific examples later in the paper. Hence, even though the calculated ΔE may differ from the experimental transition energy by a few per cent due to the finite basis set and the well known limitations of LDA-DFT, the errors involved are of the same magnitude and the combined spectra is accurate for comparison with the measured data.

Fifth, the supercell-OLCAO method is very versatile and can be applied to almost all elements in the periodic table and for any edges deep or shallow. It can be applied to almost any materials systems whether it is a metal or an insulator, an inorganic crystal or a biomolecule, having an open structure or a compact one, whether it contains numerous light atoms such as H or Li, or heavy atoms such as Y or rare earth elements. The method avoids the use of atomic radii in any parts of the calculation which could be problematic if the system under study is a complex one with different local bonding for the same element. For example, in spinel silicon nitride (γ-Si_3N_4), Si occupies both the tetrahedral and the octahedral sites in the lattice and will not have the same atomic radius. In calculations involving grain boundary (GB) models, the atoms near the GB will have very different local bonding environments than those in the bulk region. These points will be illustrated and discussed in the next section.

Sixth, because of the use of local atomic orbitals and the efficient evaluation of multi-center integrals in the analytic forms described in section 2, the method is highly efficient and can be applied to large systems. The computational demand for large complex systems in the supercell-OLCAO method comes from two sources. The first one is from the calculation of all multi-center integrals in the setup stage. In this respect, it should be pointed out that the OLCAO method is essentially an order N method in the evaluation of the Hamiltonian and overlap matrices since localized atomic orbitals are used in the basis. The judicious choice of a fixed set of Gaussian exponentials $\{\alpha_j\}$ in (3) for different orbital wave functions of the same atom and the strategy to represent the total potential function using the atom-centered Gaussian functions in (7) have significantly reduced the total number of three-center integrals that need to be evaluated. The second part is from the diagonalization of the full secular equation (an order N^3 process) in the self-consistent iterations which always use the FB, and in the calculation of the initial and final states for the final spectrum which may employ the EB. Currently, calculations have been applied to a $\Sigma 31$ GB model in alumina with 700 atoms and to a model of water with 320 H_2O molecules (1020 atoms). These results will be presented in section 4.

3. Review of past calculations using the supercell-OLCAO method

Over the last eight years, a large number of XANES/ELNES spectral calculations for complex oxides and nitrides have been performed using the supercell-OLCAO method with results in very good agreement with experiments. These calculations were carried out almost exclusively by the electronic structure group (ESG) at the University of Missouri–Kansas City (UMKC) and the group at Kyoto University and more recently at the University of Tokyo in Japan. They include a large number of crystals with simpler structures [23, 43–56], crystals with more complex structures [57–63], crystals with anisotropy [52, 54], crystals containing defects [64–69], surfaces [70], interfaces [71], grain boundaries [64, 72–74, 68], solid solutions [75], high T_c superconductors [73, 76], and more. Some of these results have been reviewed by Tanaka *et al* [29]. We will selectively comment on some of these recent calculations focusing mostly on the more complex crystals and structures.

Figure 3 shows a non-polar $\{122\}\sum = 9$ GB model in β-SiC [72]. To maintain periodic boundary conditions for the calculation, the model contains two equivalent but oppositely oriented GBs. The special feature of this model is the presence of the so-called Si–Si and C–C 'wrong bonds' in SiC due to the creation of the 5-member and 7-member rings at the GB. Such GBs have been observed in HRTEM images in CVD SiC films [77]. The wrong Si–Si (C–C) bonds in this model have bond lengths increased (decreased) by 19.1% (23.1%) from the Si–C bond length in β-SiC. The bond angles for atoms near the GB are also severely distorted [72]. Such wrong bonds result

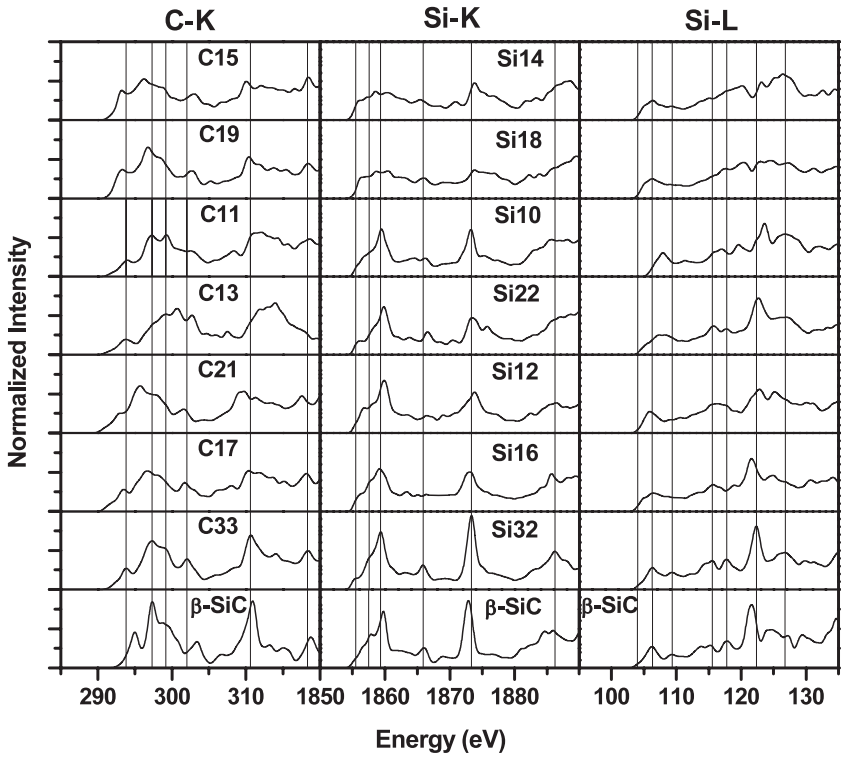

Figure 4. Calculated C K, Si K, Si L_3 edges in the non-polar SiC GB model for selected atoms as indicated. (see text for details). The corresponding spectra from the bulk crystalline b-SiC are shown in the lowest panels. The C K edge for β-SiC is shifted by 3.41 eV to match the absorption edge.

in different electronic structures and XANES/ELNES spectra. Figure 4 shows the calculated C K, Si K, and Si L_3 edges for selected wrong bond atoms (Si14, Si18, C15, C19), GB region atoms (Si10, Si22, Si12, S16, C11, C13, C21, C17), and bulk crystal region atoms (Si32, C33). Also shown at the bottom of figure 4 are the corresponding C K, Si K, and Si L_3 edges obtained from the supercell calculation in perfect β-SiC crystal. It can be seen that the wrong bonded atoms have spectra that are quite different from those of the bulk atoms. Further, even the spectra of those atoms in the GB region that do not have the wrong bonds deviate slightly from those in the bulk region because of the large bond angle variations. This clearly indicates that the XANES/ELNES spectra of atoms depend critically on their local bonding environments. On the other hand, the spectra for atoms in the bulk region agree with those in the perfect crystal, as expected. Similar results for the same GB but with polar interfaces are also calculated with similar conclusions [72]. Recent developments in microscopy technology will enable such spectral differences to be observed directly.

Another interesting example is the XANES/ELNES spectral calculation of the three phases of $AlPO_4$ which are formed at different pressures [58]. The most well known phase is α-$AlPO_4$ (berlinite) with a trigonal structure that is isostructural with α-quartz. In α-$AlPO_4$, both Al and P are tetrahedrally coordinated with O with Al–O bond lengths of 1.727 and 1.728 Å and P–O bond lengths of 1.518 and 1.524 Å. At a pressure of 13 GPa, it transforms into an orthorhombic phase (o-$AlPO_4$) in which Al ions become octahedrally coordinated (Al–O bond lengths 1.818, 1.913 Å) but the P ions remain tetrahedrally coordinated (P–O bond lengths 1.463, 1.576 Å). At an even higher pressure of 97.5 GPa, $AlPO_4$ transforms into a monoclinic phase (m-$AlPO_4$) in which both Al and P are octahedrally coordinated with Al–O bond lengths of 1.716 and 1.745 Å and P–O bond lengths of 1.503 and 1.879 Å. This was the first time the presence of six-fold coordinated P has been reported [78]. The interesting point is that these three phases of $AlPO_4$ offer a rare example of structurally different crystals with the same formula unit, the same number of different types of ions, but similar local units among them. According to the prevailing notion of the so-called 'fingerprinting' technique, the XANES/ELNES spectra of an ion can be predicted by the local nearest neighbor (NN) coordination. However, the supercell-OLCAO calculation shows that this is not true [58]. Figure 5 compares the calculated Al K and Al L3 edges of the octahedrally bonded Al in o-$AlPO_4$ and m-$AlPO_4$. Figure 6 compares the P K and P L_3 edges of the tetrahedrally bonded P in α-$AlPO_4$ and o-$AlPO_4$. Figure 7 compares the O K edges of O1 site in o-$AlPO_4$ and O2 site in m-$AlPO_4$, both are three-fold bonded to two Al and one P. None of these comparisons support the widely used 'fingerprinting' interpretation technique. The only experimental data we can locate is the P K edge in α-$AlPO_4$ [79] which is in good agreement with the calculations.

Similar conclusions on the non-validity of the 'fingerprinting' technique have been reached in extensive calculations in ten crystals in the Y–Si–O–N system which provides a large data base for analysis [59]. The O K, N K, Si K, Si L_3, Y K, and Y L_3 edges in six binary (α-SiO_2, stishovite SiO_2, β-Si_3N_4, α-Si_3N_4, γ-Si_3N_4, Y_2O_3),

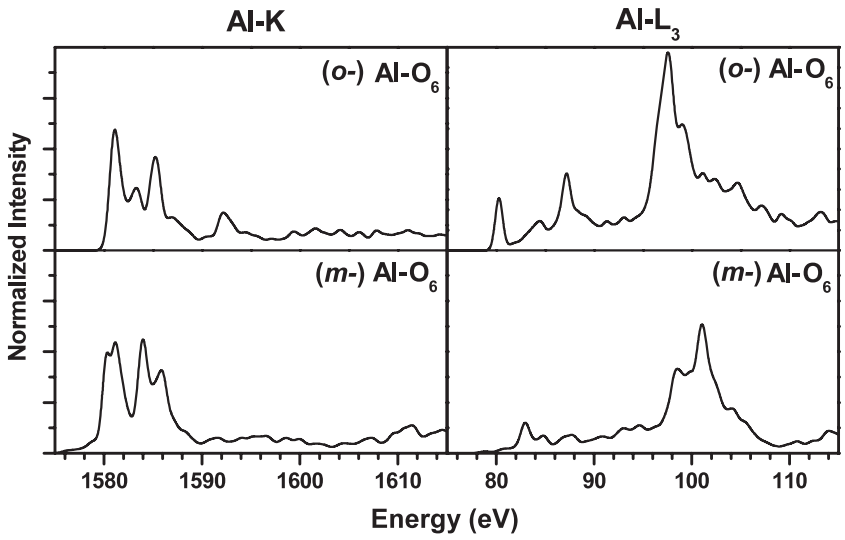

Figure 5. Comparison of the Al K and Al L3 edges for octahedrally bonded Al in o-$AlPO_4$ and m-$AlPO_4$.

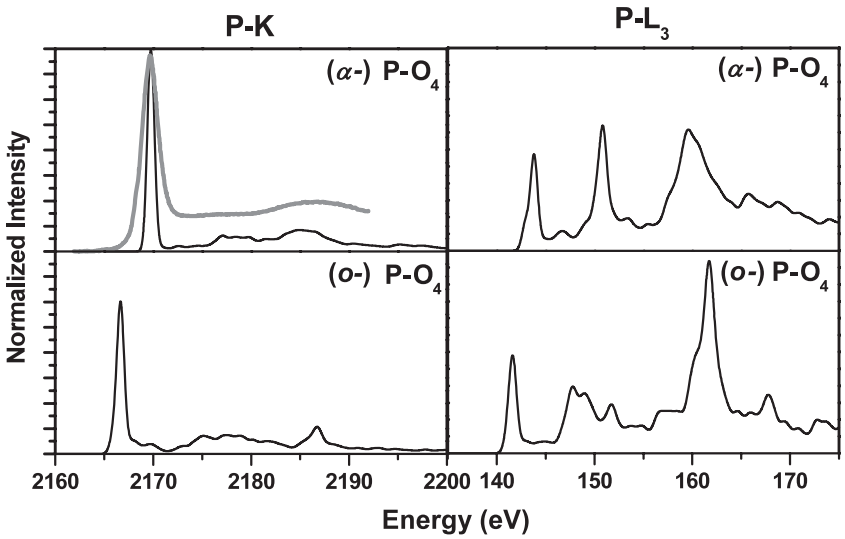

Figure 6. Comparison of the P K and P L_3 edges for tetrahedrally bonded P in α-$AlPO_4$ and o-$AlPO_4$.

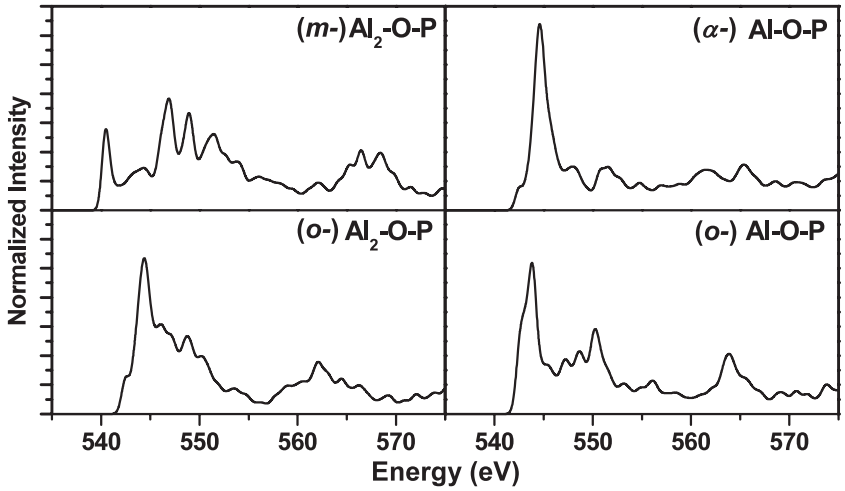

Figure 7. Comparison of the O K edges of 3-fold bonded O in m-$AlPO_4$ and o-$AlPO_4$.

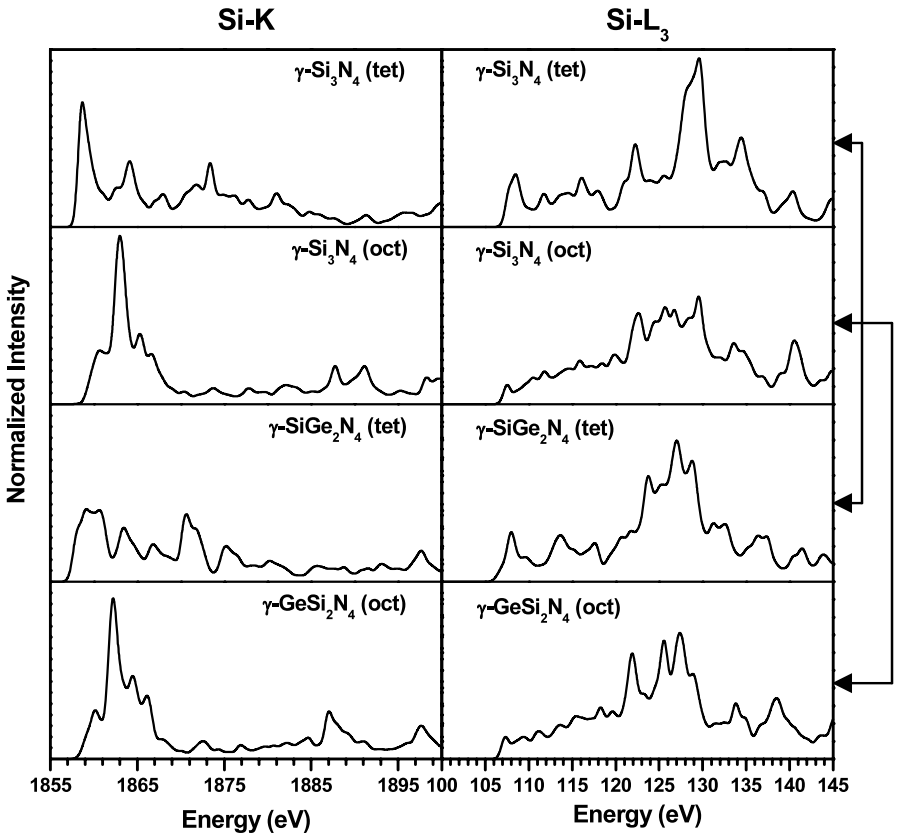

Figure 8. Calculated Si K and Si L_3 edges in the four spinel nitrides. The arrows pair up the cases for Si in the tetrahedral site and in the octahedral site of the spinel lattice.

three ternary (Si_2N_2O, $Y_2Si_2O_7$, Y_2SiO_5) and three quaternary ($Y_2Si_3N_4O_3$, $Y_4Si_2O_7N_2$, $Y_3Si_5N_9O$) crystals were calculated using the supercell-OLCAO method and carefully analyzed. No meaningful correlation can be established between spectral features on the calculated spectra and the atomic environment based on the NN coordination.

Other notable accomplishments of the supercell-OLCAO calculation include the application of the calculation to identify ultra dilute dopants in MgO [65], the faithful reproduction of the anisotropy in wurtzite crystals [52, 54] and the elucidation of the structure of γ-Al_2O_3 [60]. More recently, calculations on metal–ceramic interfaces [71] and high T_c superconductors $YBa_2Cu_3O_7$ (YBCO) [63, 76] were also reported. The O K edges for atoms at the Cu/Al_2O_3 heterointerface were calculated and its dependence on the direction of momentum transfer was discussed. It was demonstrated that the O K edges from four different types of O in YBCO are very different and only the weighted sum compares favorably with the measured data. The remarkable part of this paper was the ability to resolve the bonding for O ions in the Cu–O chain and that in the Cu–O planes. This indicates the great versatility of the supercell-OLCAO method emphasized in the last section.

4. Select results from recent calculations

In this section, we present some as yet unpublished new results on XANES/ELNES calculations using the supercell-OLCAO method which can further exemplify the strengths of this method.

4.1. Binary and ternary spinel nitrides

The successful synthesis of Si_3N_4 in the cubic spinel structure (γ-Si_3N_4) in 1999 [80] has lead to many theoretical and experimental studies of spinel nitrides [81–83]. Three binary spinel nitrides γ-Si_3N_4, γ-Ge_3N_4, γ-Sn_3N_4, have been successfully synthesized [84–86]. Many of the early XANES/ELNES calculations using the supercell-OLCAO method were on these compounds [44, 47, 49, 50, 75] because of the unique feature that the same cation occupies both the tetrahedral A site and the octahedral B site of the spinel lattice. The only ternary compound that has been studied in considerable detail is the spinel nitride with Si and Ge as cations [87, 88]. Several calculations on the structure and properties of Si/Ge spinel nitrides have been carried out [88–91]. In an earlier calculation, Ching *et al* predicted that γ-$GeSi_2N_4$ is unstable or meta-stable while γ-$SiGe_2N_4$ should be stable [90]. This is in line with the conventional expectation that the smaller Si ion should prefer the smaller tetrahedral site and the larger Ge ion would prefer the larger octahedral site. However, experimental findings showed a composition close to γ-$GeSi_2N_4$ [87] which appears to be counter intuitive. Further investigation on the relative stabilities of these compounds point to the possible existence of a solid solution series of γ-$(Si_xGe_{1-x})_3N_4$ [92–94]. Because

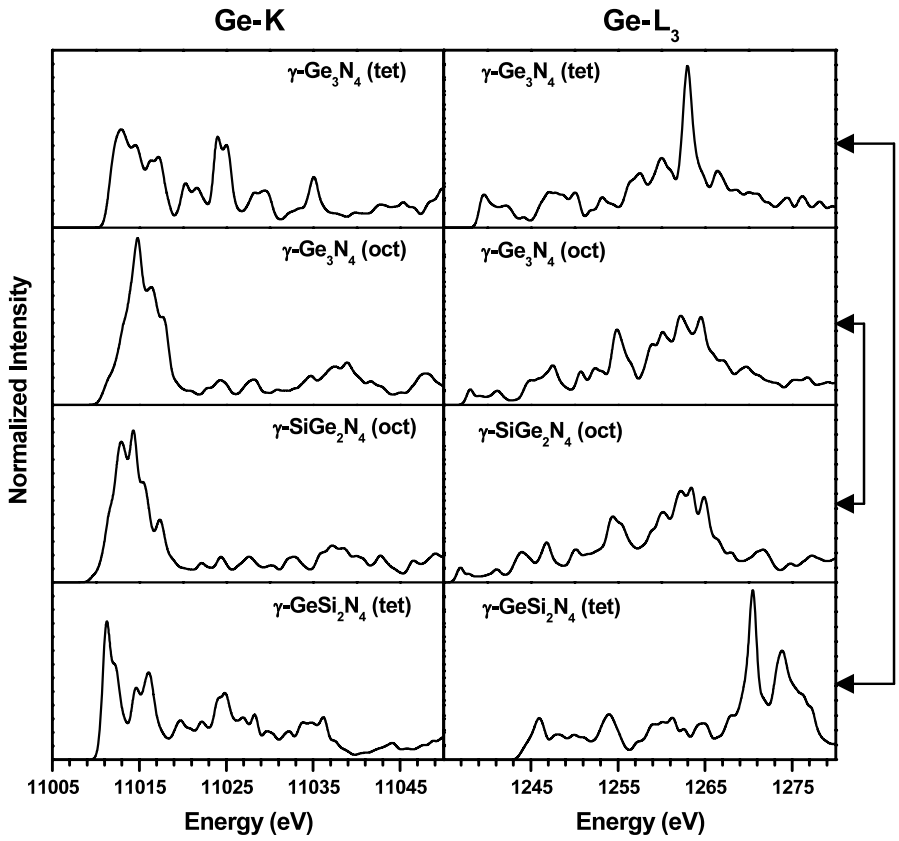

Figure 9. Calculated Ge K and Ge L_3 edges in the four spinel nitrides. The arrows pair up the cases for Ge in the tetrahedral site and in the octahedral site of the spinel lattice.

of the possible disordered nature of the compound and the fact that single crystals of sufficient size are not available, XANES/ELNES spectra may be a useful technique to resolve some of these controversies. To this end, we have calculated and compared the XANES/ELNES spectra in the four spinel nitrides: γ-Si_3N_4, γ-Si_3N_4, γ-$SiGe_2N_4$, and γ-$GeSi_2N_4$. The structures of these four compounds were first optimized using the Vienna *ab initio* simulation package (VASP) [95, 96]. The K- and L-edges for cations at the tetrahedral and octahedral sites are calculated using the supercell-OLCAO method and compared. Also calculated are the N K edges in the four crystals.

Figure 8 shows the calculated Si K and Si L_3 edges in the four crystals. When we compare the spectra of the Si K and Si L_3 edges for Si at the tetrahedral site in γ-Si_3N_4 and γ-$SiGe_2N_4$ it is apparent that there are no similarities, especially for the Si K edge. Similarly, we compared the Si K and Si L_3 edges for Si at the octahedral site in γ-Si_3N_4 and γ-$GeSi_2N_4$. Here there are similarities especially in the Si K edge. It is not clear as to why there are such differences for Si at the two different sites in the four spinel nitrides. Figure 9 shows similar comparisons for the Ge K and Ge L_3 edges. Again there are little resemblances in Ge K and Ge L_3 edges for Ge at the tetrahedral site in γ-Ge_3N_4 and γ-$GeSi_2N_4$ although the dissimilarities are less than that for the Si K and Si L_3 edges in figure 8. Similarly, the Ge K and Ge L_3 edges for Ge at the octahedral sites in γ-Ge_3N_4 and γ-$SiGe_2N_4$ show some degree of similarities. A possible explanation is that when a cation is at the smaller site, its interaction with atoms beyond the NN coordination shell becomes more important and its XANES/ELNES spectra show a greater degree of variation. On the other hand, the N K edges in the four spinels (figure 10) show unambiguous and distinctively different features. Since there is only one unique site for N in the spinel nitrides, it appears that the use of the theoretical N K edge spectra to interpret an experimentally measured one will likely be effective in identifying the correct phase in the ternary spinel nitrides. The calculated N K edge in γ-Si_3N_4 has already been shown to agree with the experiment [49]. Within the first 25 eV from the edge on-set, γ-$SiGe_2N_4$ has two prominent peaks A and B and a smaller peak C. On the other hand, γ-$GeSi_2N_4$ shows four well-resolved peaks A′, A, B, and C within the same energy range with C being the most prominent. Also, the N K edge in γ-$GeSi_2N_4$ has a steeper on-set slope than that in γ-$SiGe_2N_4$. The real samples in ternary spinel nitrides may also contain additional impurities or vacancies that could add to the uncertainty in the measured spectra and make them even more difficult to interpret.

4.2. Y K edges in Y-doped Σ31 *GB in* Al_2O_3

It is well known that Y impurities in alumina tend to segregate to the GBs in polycrystalline alumina and can increase the creep resistance. Using scanning transmission electron microscopy (STEM) and bicrystals of Al_2O_3 doped with Y,

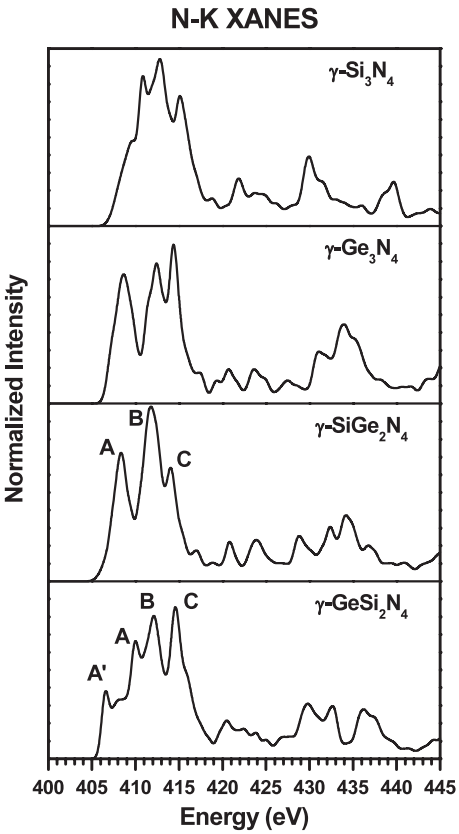

Figure 10. Calculated N K edges in the four spinel nitrides.

it was clearly shown that, in the case of the Σ31 GB, Y segregates to the center of the 7-member rings of Al columns [10]. Based on *ab initio* theoretical simulations, the strengthening of the Y segregated Σ31 GB in alumina was explained as being due to the increased number of Y–O bonds and their strength compared to the Al–O bonds they replace. The Σ31 GB model in that study has 700 atoms and contains two oppositely oriented GBs due to the periodic boundary conditions. The system is sufficiently large to serve as a supercell for the supercell-OLCAO calculation. Recently, we have calculated the Y K edge of the Y ion at the center of the seven-member rings of Al columns. The calculated result is displayed in figure 11. Also shown are the Y K edges from three other different systems: crystalline Y_2O_3 in the bixbyte structure, Yttrium alumina garnet (YAG) in the garnet structure, and the YBCO superconductor in the perovskite structure. The supercell sizes in these three cases are respectively 80, 160, and 117 atoms. As can be seen, the Y K edges in these four cases are completely different because of the very different local environment of Y. In the Σ31 GB, Y is bonded to six different O ions with bond lengths ranging from 2.14 to 3.00 Å. In Y_2O_3 there are two different Y sites, both of which are six-fold coordinated with slightly different bond lengths ranging from 2.29 to 2.39 Å. In YAG, Y is 8-fold coordinated with two bond lengths of 2.30 and 2.43 Å. In YBCO, Y is also eight-fold coordinated with Y–O bond lengths of 2.39 and 2.41 Å, similar to that in YAG. The large differences in these spectra, especially in the case of Y in the Σ31 GB and in YBCO underscore the sensitive dependence of the XANES spectrum of an ion to its local environment, not just in the number and type of NN atoms and their bond lengths, but also the presence of other ions beyond the NN atoms such as in the YBCO superconductor. Such investigations for materials with complex structures are only in the beginning stages and more such studies are expected.

4.3. Two-dimensional carbon structures

One of the earliest XANES/ELNES studies was on the C K edge in graphite which clearly showed two sharp peaks above the absorption edge and labeled them as π^* and σ^* to serve as fingerprints for two-dimensional sp^2 bonding in carbon systems. These have been extremely useful, especially in organic and bio-related materials characterization. However, little has been discussed concerning the structures in the C K edge other than these two peaks. In figure 12, we compare the calculated C K edges in five sp^2 bonded C systems: graphite, graphene, and three single walled carbon nanotubes (SWCNT) labeled as $[n, m,$ (s, m)] where n and m are integers denoting the relative positions of the circumferential vector when a graphene sheet is rolled onto itself in forming the SWCNT [97, 98] and s or m indicate whether it is a semiconductor or a metal. The three SWCNTs are: [4, 2, s] with a radius 2.071 Å, [9, 3, m] with a radius 4.234 Å, and [14, 0, s] with a radius 5.480 Å. As can be seen, the five spectra are indeed very similar showing characteristic π^* and σ^* peaks at almost the same energy. However, on a closer inspection, one can see small difference in the spectra above 10 eV from the edge on-set. The difference is quite small between graphene and graphite since graphene is just a single sheet of graphite and the effect of interlayer coupling is obviously small. Still there are obvious differences in the numbers and locations of peak structures at energies 15 eV above the absorption edge. The differences in the C K edge with the SWCNTs are more significant. The calculations for SWCNT were done with the model containing a single tube in a supercell of 20 Å × 20 Å with periodicity in z direction. The different radii of the three tubes give different strains in the 2-d wrapping of the carbon sheets and these differences show up in the different peak structures of the C K edge at energies above 10 eV from the edge on-set. A broad structure appears between the π^* and σ^* peaks in the small radius [4, 2, s] tube and disappears in the larger radius [14, 0, s] tube. These preliminary calculations again demonstrate that the current supercell-OLCAO method is capable of delineating minute difference in the two-dimensional carbon system as reflected in the calculated C K edge spectra. When the axial and radial components of these spectra are analyzed, more distinct features can be treated.

4.4. O K edges in water molecules

Although water is the most common material on earth's surface, its structure and properties are complicated, fascinating, and the subject of many experimental and theoretical studies. Surprisingly, there have not been extensive data obtained via XANES/ELNES measurement. Recently, Iannuzzi published

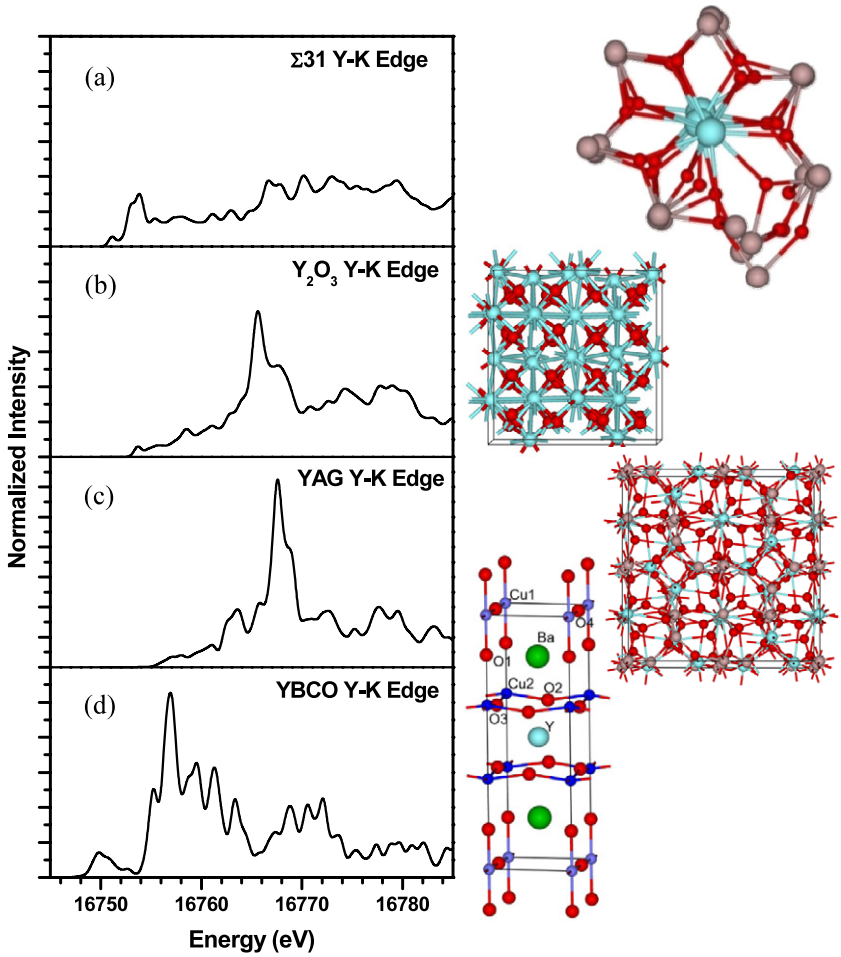

Figure 11. Comparison of the calculated Y K edges in four systems. (a) Y at the core of the Σ31 GB in alumina; (b) Y_2O_3; (c) $Y_3Al_5O_{12}$ (YAG); and (d) $YBa_2Cu_3O_7$ (YBCO). The structures of these four systems are sketched at the right.

a calculation on the O K edge for water molecules using an all-electron Gaussian and augmented plane wave calculation [99]. The result was not in particularly good agreement with experiment [100] and the implication of the H bonding between water molecules was inferred. We have used the supercell-OLCAO method to calculate the O K edge of water molecules. The model we used is a cubic cell with 340 H_2O molecules (1020 atoms) with a density of 1gm/cc. The model was constructed using an *ab initio* molecular dynamic code [101] and is a part of an overall investigation on the electronic structure and optical properties of water. Since water is a liquid with an amorphous structure with random orientations determined by H bonding, other short-range and long-range interactions [102], none of the H_2O molecules and hence O atoms in the water molecule should have the same local environment and their O K edges will not be the same. This is indeed the case. Figure 13 shows the calculated O K edges of 10 different O ions in the model and their average. Also shown are the experimental data from [100] for comparison (calculated curve shifted by −5.22 eV to align the major peak). As can be seen, the 10 individual O K edges from the calculation are very different and bear little resemblance to the experimental spectrum. These O ions in water molecules have different numbers H bonds and bond distances with other water molecules. However, the averaged spectrum is very close to the measured one in terms of the peak shape and other minor structures. The calculated spectrum covers a much wider range of energy than the measured data, presumably due to experimental difficulties with liquid samples. This is another example of using theoretical calculations to supplement the data where laboratory measurements may be difficult to carry out.

4.5. Co K edge in vitamin B_{12}

In recent years, XANES/ELNES spectroscopic studied have found many applications to bio-inspired materials [103–105]. We would like to explore the possibility of using the supercell-OLCAO method for such studies. The OLCAO method has been successfully used to study the electronic structure and bonding in B_{12} cobalamins [106–109]. This includes the cyanocobalamin (CNCbl), methylcobalamin (MeCbl), adenosylcobalamin (AdoCbl) and hydroxocobalmin (OHCbl). The central focus is the octahedral Co(III) ion at the center of the corrin ring to which the cofactor R (R = CN, NH_3, Ado, or OH) attaches in the sixth position. All the currently known reactions of the B_{12}-dependent enzymes involves the making or breaking of the Co–C bond between R and Co. Champloy *et al* have published the x-ray absorption spectra

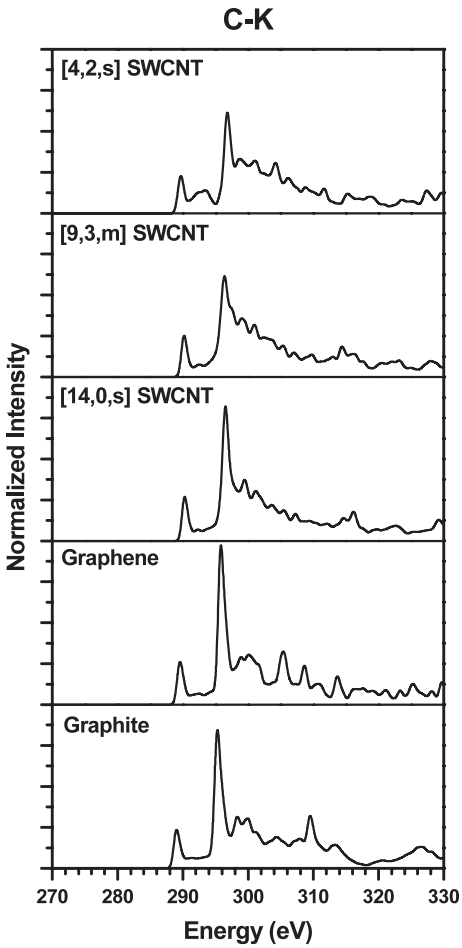

Figure 12. Calculated C K edges in three SWCNT compared with C K edge of graphene and graphite.

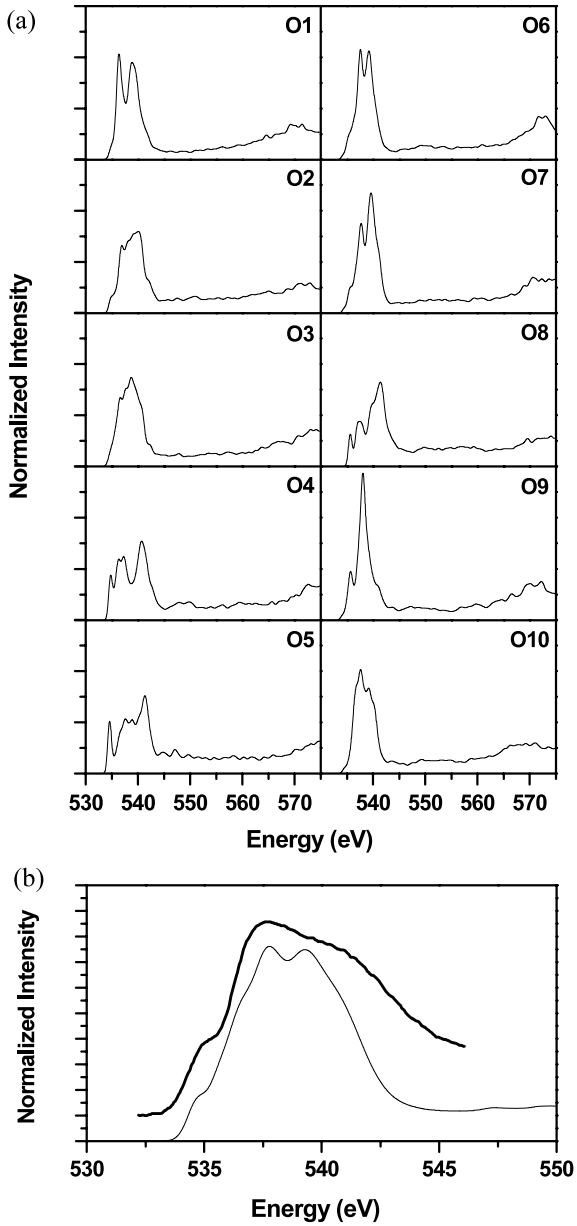

Figure 13. (a) Calculated O K edges in 10 different water molecules; (b) the averaged O K edges in (a) shifted by −5.22 eV. The dashed line is the experimental curve from [100].

of these cobalamins [110]. The motivation of that study was to investigate whether the bond elongation to Co is due to the x-ray induced reduction of the cofactor's Co center. To this end, the Co K-edges of these cobalamins before and after radiation were measured. Figure 14 shows the result of our preliminary calculation of the Co K edge in CNCbl together with the measured data of CNCbl before irradiation from [110]. Also shown in figure 14 is the structure of the vitamin B_{12} molecule in the supercell. In spite of the low experimental energy resolution, there is a very decent agreement with the calculated spectrum. Not only the double peak structure and its slope are faithfully reproduced, also in agreement is the presence of two pre-peaks between 7670 and 7680 eV and some other minor structures in the spectrum. This gives us a great confidence in using the supercell-OLCAO method to calculate the XANES/ELNES spectra in complex biomaterials and biomolecules.

5. Conclusions

We have reviewed the supercell-OLCAO method for *ab initio* XANES/ELNES calculation in a variety of materials systems. The theory and the techniques of this method are fully described and special advantages of the method pointed out. From these results, several major conclusions emerge.

(1) In complex crystals and non-crystalline materials, there would be many nonequivalent atomic sites for a given element. In these cases, the weighted average of the spectra from different sites should be used to compare with the measured ones. Depending on the actual variations of their local environment, these spectra can differ widely and so will their final weighted sum.

(2) The often celebrated fingerprinting technique based on local NN coordination of an ion to interpret the experimental data should be dismissed. There is no basis for such simple interpretation except in a small set of limited cases with single elements and simple structures.

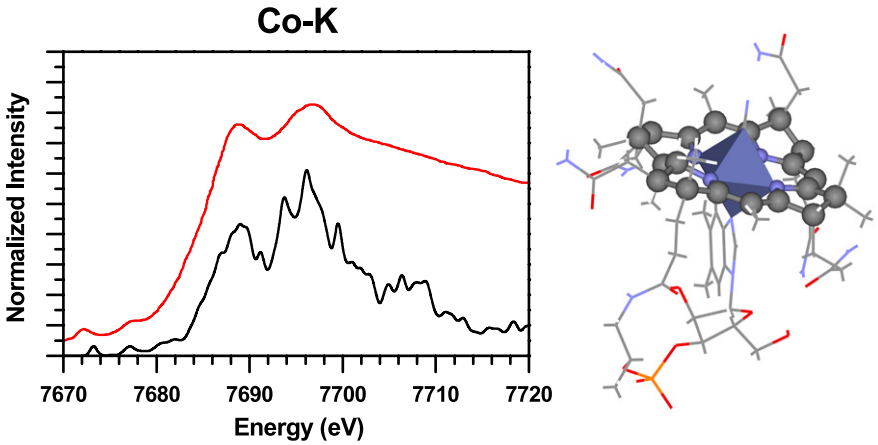

Figure 14. Calculated Co K edge in CN–Cbl. The upper curve is the measured XAS data from [110].

The fingerprinting notion is totally untenable in complex systems. A common argument of using the fingerprinting technique is that they reflect the oxidation state of the ion. However, the assignment of oxidation state or the charged state with an integer value is increasingly under attack [111] on the grounds of detailed calculations that show it to be a myth due to charge self-regulation [112].

(3) The main purpose of XANES/ELNES calculation is for the characterization of structurally complicated systems such as those involving defects, interfaces, or grain boundaries where experimental investigations face many challenges and where their interpretations are difficult. However, spectral calculation of structurally complicated multi-component systems can be overwhelming and intractable. In our opinion, the best strategy would be to carefully model the anticipated structure through large-scale structural modeling, (equivalent to experimental theoretical sample preparations), accurately calculate the XANES/ELNES spectra of atoms of interest and then compare with experiments to assess the validity of the model constructed.

In spite of the many advantages of the supercell-OLCAO method, there are still ample grounds for improvement. For example, at present the $L_{2,3}$ edges of the transition metals cannot be calculated because the spin–orbit interaction is not included in the present method. A proper treatment may require the inclusion of multiplet effects [113, 114]. For magnetic oxides, the underlying LDA theory may have to be extended to account for the intra-atomic correlations. There are also cases where the agreement between experiment and calculation is not always satisfactory, and it is not clear if there are some fundamental limitations in the method or it is related to the experimental measurement such as the nature of the samples used. In certain materials systems where the dipole transition is forbidden or weak, it would be necessary to extend the calculation beyond the dipole approximation [115, 116]. There are also questions about putting the excited electron from the core level in the bottom of the conduction band in the supercell-OLCAO method. Is this the best description of what happens in the experimental process? Perhaps it would be more realistic to spread the excited electron through the entire CB region. This is particularly important for applications to biological systems since there will be only excited energy levels, not the conduction bands, and the proper placement of the excited electron is important for the accuracy of the final spectrum. Such possibilities are certainly worth pursuing. Another issue worth considering is the proper development of the energy-dependent broadening procedure to account for the life-time broadening which could potentially improve the agreement with measured data. Given time and resources, these are not insurmountable obstacles.

In summary, we believe that the supercell-OLCAO method has great potential for further development and greater applications. For example, the generalization to a spin-polarized version [22] and with the inclusion of spin–orbital splitting the method can be very competitive for x-ray magnetic circular dichroism calculations for the $L_{2,3}$ edges in magnetic systems which can now be accessed by modern TEM [117]. Currently, the supercell-OLCAO method has only been applied to transitions from the core to the CB. With some diligence, calculations can be extended to resonant and non-resonant inelastic scattering processes in general including the x-ray emission spectra (XES) and soft x-ray fluorescence spectroscopy where many experimental data exist [118, 119]. Another very promising area is to develop a spectral imaging technique based on the calculated spectral data that can complement the experimental imaging using modern microscopy [120]. However, the greatest opportunity for the supercell-OLCAO method is with biomaterials and biomolecules where the structures are much more complicated and the need for theoretical input is urgent. The localized orbital description for the electronic structure in such systems is most natural. The preliminary data on O K edges in water molecules and Co K edge in cyanocobalamin show great encouragement in this direction.

Acknowledgments

This research is support by the US Department of Energy under the Grant No. DE-FG02-84DR45170. This research used the

resources of NERSC supported by the Office of Science of DOE under the contract No. DE-AC03-76SF00098.

References

[1] Koningsberger D C and Prins R (ed) 1988 *X-Ray Absorption: Principles, Applications,Techniques of EXAFS, SEXAFS, and XANES* (*Chemical Analysis* vol 92) (New York: Wiley)
[2] Chen J G 1997 *Surf. Sci. Rep.* **30** 1–152
[3] Stöhr J 1992 *NEXAFS Spectroscopy* (Berlin: Springer)
[4] Disko M M, Ahn C C and Fultz B (ed) 1992 *Transmission Electron Energy Loss Spectrometry in Materials Science* (Warrendale, PA: The Minerals, Metals and Materials Society)
[5] Egerton R F 1996 *Electron-Energy Loss Spectroscopy in the Electron Microscope* 2nd edn (New York: Plenum)
[6] Urban K W 2008 *Science* **321** 506
[7] Pennycook S J, Varela M, Hetherington C J D and Kirkland A I 2006 *MRS Bull.* **31** 36–43
[8] Kimoto K, Asaka T, Nagai T, Saito M, Matsui Y and Ishizuka K 2007 *Nature* **450** 702–4
[9] Muller D A, Kourkoutis L F, Murfitt M, Song J H, Hwang H Y, Silcox J, Dellby N and Krivanek O L 2008 *Science* **319** 1073–6
[10] Buban J, Matsunaga K, Chen J, Shibata N, Ching W Y, Yamamoto T and Ikuhara Y 2006 *Science* **311** 212–5
[11] Parallel total energy code (PARATEC) (WWW.NERSC.gov/projects/paratec)
[12] Natoli C R, Misemer D K, Doniach S and Kutzler F W 1980 *Phys. Rev.* A **22** 1104
Hatada K, Hayakawa K, Benfatto M and Natoli C R 2007 *Phys. Rev.* B **76** 060102
[13] Blaha P, Schwarz K, Madsen G, Kvasnicka D and Luitz J 2001 *Computer code Wien2K, An Augmented Plane Wave + Local Orbital Program for calculating Crystal properties* K. Schwaz, Techn. Universität Wien, Austria
[14] Shirley E L 1998 *Phys. Rev. Lett.* **80** 794
Rohlfing M and Louie S G 1998 *Phys. Rev. Lett.* **80** 3320
[15] FEFF8 an automated program for *ab initio* multiple scattering calculations of x-ray Absorption Fine Structure (XAFS) and x-ray Absorption Near-Edge Structure (XANES) spectra for clusters of atoms http://leonardo.phys.washington.edu/feff/
[16] Tanaka I 2009 *J. Phys.: Condens. Matter* **21** 104201
[17] Slater J C and Koster G F 1954 *Phys. Rev.* **94** 1498
[18] Ching W Y 1990 *J. Am. Ceram. Soc.* **73** 3135–60
[19] Ching W Y and Lin C C 1975 *Phys. Rev.* B **12** 5536
[20] Herring C 1940 *Phys. Rev.* **57** 1169
[21] Mullikan R S 1955 *J. Am. Chem. Soc.* **23** 1833
Mullikan R S *J. Am. Chem. Soc.* **23** 1841
[22] Ching W Y 1995 *The Magnetism of Amorphous Metals and Alloys* ed J A Fernandez-Baca and W Y Ching (Singapore: World Scientific) p 85
[23] Mo S-D and Ching W Y 2000 *Phys. Rev.* B **62** 7901–7
[24] Schattschneider P 1989 *Ultramicroscopy* **28** 1
[25] Fuggle J C and Inglesfield J E (ed) 1992 *Unoccupied Electronic States, Fundamentals for XANES, EELS, IPS and BIS* (New York: Springer)
[26] Muller D A, Singh D J and Silcox J 1998 *Phys. Rev.* B **57** 8181–202
[27] Rehr J J and Alberts R C 2000 *Rev. Mod. Phys.* **72** 621–54
[28] Brühwiler P A, Katris O and Mårtensson N 2002 *Rev. Mod. Phys.* **74** 703
[29] Tanaka I, Mizoguchi T and Yamamoto T 2005 *J. Am. Ceram. Soc.* **88** 2013–29
[30] de Groot F and Kotani A 2008 *Core Level Spectroscopy of Solids* (Boca Raton, FL: CRC press)
[31] Dirac P A M 1927 *Proc. R. Soc.* A **114** 243–65
[32] Hjalmarson H P, Buttner H and Dow J D 1980 *Phys. Rev.* B **24** 6010–9
[33] Weijs D J W *et al* 1990 *Phys. Rev.* B **41** 11899–910
[34] Tanaka I and Adachi H 1996 *Phys. Rev.* B **54** 4604–8
[35] Zannen J, Sawatzky G A, Fink J, Speier W and Fuggle J C 1985 *Phys. Rev.* B **32** 4905–13
[36] Tamura E, van Ek J, Fröba M and Wong J 1995 *Phys. Rev. Lett.* **74** 4899–902
[37] Lindner Th, Sauer H, Engel W and Kambe K 1986 *Phys. Rev.* B **33** 22–4
[38] Robertson J 1983 *Phys. Rev.* B **6** 3378–85
[39] Tanaka I and Adachi H 1996 *Phys. Rev.* B **54** 4604
[40] Mizoguchi T, Tanaka I, Yoshiya M, Oba F, Ogasawara K and Adachi H 2000 *Phys. Rev.* B **61** 2180
[41] Hohenberg P and Kohn W 1964 *Phys. Rev.* **136** 864–71
[42] Kohn W and Sham L J 1965 *Phys. Rev.* **140** A1133–8
[43] Mo S-D and Ching W Y 2001 *Appl. Phys. Lett.* **78** 3809–11
[44] Ching W Y, Mo S-D and Chen Y 2002 *J. Am. Ceram. Soc.* **85** 11–5
[45] Ching W Y, Ouyang L, Rulis P and Tanaka I 2005 *Phys. Status Solidi* b **242** R94–6
[46] Ching W Y, Xu Y-N, Rulis P and Ouyang L 2006 *Mater. Sci. Eng.* A **422** 147–56
[47] Ching W Y and Rulis P 2006 *Phys. Rev.* B **73** 045202
[48] Aryal S, Rulis P and Ching W Y 2008 *Am. Mineral.* **93** 114–23
[49] Tanaka I, Mizoguchi T, Sekine T, He H, Kimoto K, Mo S-D and Ching W Y 2001 *Appl. Phys. Lett.* **78** 2134–36
[50] Tanaka I, Oba F and Ching W Y 2001 *Mater. Integr.* **14** 21–6
[51] Mizoguchi T, Tanaka I, Kunisu M, Yoshiya M, Adachi H and Ching W Y 2003 *Micron* **34** 249–54
[52] Mizoguchi T, Tanaka I, Yoshioka S, Kunisu M, Yamamoto T and Ching W Y 2004 *Phys. Rev.* B **70** 045103
[53] Suga T, Mizoguchi T, Kunisu M, Tatsumi K, Yamamoto T, Tanaka I and Sekine T 2004 *Mater. Trans.* **45** 2039–41
[54] Suga T, Kameyama S, Yoshioka S, Yamamoto T, Tanaka I and Mizoguchi T 2005 *Appl. Phys. Lett.* **86** 1631135
[55] Mizoguchi T, Sakurai M, Nakamura A, Sasaki T, Sato Y, Matsunaga K, Yamamoto T and Ikuhara Y 2005 *Mater. Sci. Forum* **475–479** 3119–22
[56] Mizoguchi T, Tatsumi K and Tanaka I 2006 *Ultramicroscopy* **106** 1120–8
[57] Xu Y-N, Chen Yu, Mo Shang-Di and Ching W Y 2002 *Phys. Rev.* B **65** 235105
[58] Ching W Y and Rulis P 2008 *Phys. Rev.* B **77** 125116
[59] Ching W Y and Rulis P 2008 *Phys. Rev.* B **77** 35125
[60] Ching W Y, Ouyang L, Rulis P and Yao H 2008 *Phys. Rev.* B **78** 014106
[61] Hussain A, Aryal S, Rulis P, Choudhry M S and Ching W Y 2008 *Phys. Rev.* B **78** 195102
[62] Kimoto K, Matsui Y, Nabatame T, Yasuda T, Mizoguichi T, Tanaka I and Toriumi A 2003 *Appl. Phys. Lett.* **83** 4306–8
[63] Mizoguchi T, Varela M, Buban J P, Yamamoto T and Ikuhara Y 2008 *Phys. Rev.* B **77** 024504
[64] Ching W Y, Rulis P, Chen Y and Kohyama M 2006 *Interfaces in Electronic Ceramics* ed L Cook, D Misra, S Mukhopadhyay, W Wong-Ng, O Leonte and K Sundaram (Pennington, NJ: The Electrochemical Society) pp 137–49
[65] Tanaka I, Mizoguchi T, Matsui M, Yoshioka S, Oba F, Adachi H, Okajima T, Umesaki M, Ching W Y, Inoue Y, Mizuno M and Shirai Y 2003 *Nat. Mater.* **2** 541–5
[66] Mizoguchi T, Sakurai M, Nakamura A, Matsunaga K, Tanaka I, Yamamoto T and Ikuhara Y 2004 *Phys. Rev.* B **70** 153101
[67] Sato Y, Mizoguchi T, Oba F, Yodogawa M, Yamamoto T and Ikuhara Y 2005 *Appl. Phys. Lett.* **84** 5311–3

[68] Mizoguchi T, Sato Y, Buban J P, Matsunaga K, Yamamoto T and Ikuhara Y 2005 *Appl. Phys. Lett.* **87** 241920

[69] Mizoguchi T, Seko A, Yoshiya M, Yoshida H, Ching W Y and Tanaka I 2007 *Phys. Rev.* B **76** 195125

[70] Rulis P, Yao H, Ouyang L and Ching W Y 2007 *Phys. Rev.* B **76** 245410

[71] Mizoguchi T, Sasaki T, Tanaka S, Matsunaga K, Yamamoto T, Kohyama M and Ikuhara Y 2006 *Phys. Rev.* B **74** 235408

[72] Chen Y, Mo S D, Kohyama M, Kohno H, Takeda S and Ching W Y 2002 *Mater. Trans.* **43** 1430

[73] Rulis P, Ching W Y and Kohyama M 2004 *Acta Mater.* **52** 30009–18

[74] Sato Y, Mizouguchi T, Oba F, Yodogawa M, Yamamoto T and Ikuhara Y 2005 *J. Mater. Sci.* **40** 3059–66

[75] Tatsumi K, Mizoguchi T, Yoshioka S, Yamamoto, Suga T, Sekine T and Tanaka I 2005 *Phys. Rev.* B **71** 33202

[76] Mizoguchi T, Buban J P, Matsunaga K, Yamamoto T and Ikuhara Y 2006 *Ultramicroscopy* **106** 92

[77] Tanaka K and Kohyama M 2002 *Phil. Mag.* A **82** 215

[78] Pellicer-Porres J, Saitta A M, Polian A, Itie J P and Hafland M 2007 *Nat. Mater.* **6** 698

[79] Frank R and Hormes J 1995 *Physica* B **216** 85

[80] Zerr A, Miege G, Serghiou G, Schwarz M, Kroke E, Riedel R, Fuess H, Kroll P and Boehler R 1999 *Nature* **400** 340–2

[81] Mo S-D, Ouyang L, Ching W Y, Tanaka I, Koyama Y and Riedel R 1999 *Phys. Rev. Lett.* **83** 24–7

[82] Zerr A, Riedel R, Sikine T, Lowther T, Ching W Y and Tanaka I 2006 *Adv. Mater.* **18** 2933–48

[83] Kroke E and Schwarz M 2004 *Coordin. Chem. Rev.* **248** 493–532

[84] Leinenweber K, O'Keefe M, Somayazulu M S, Hubert H, McMillan P F and Wolf G H 1999 *Chem.—Eur. J.* **5** 3076

[85] Serghiou G, Miehe G, Tschauner O, Zerr A and Boehler R 1999 *J. Chem. Phys.* **111** 4659–62

[86] Shemkunas M, Wolf G H, Leinenweber K and Petuskey W T 2002 *J. Am. Ceram. Soc.* **85** 101–4

[87] Soignard E, Somayazulu M, Mao H-K, Dong J, Sankey O F and McMillam P F 2001 *Solid State Commun.* **120** 237

[88] Ching W Y, Mo S-D and Ouyang L 2001 *Phys. Rev.* B **63** 245110

[89] Ching W Y, Mo S-D, Tanaka I and Yoshiya M 2001 *Phys. Rev.* B **63** 064102

[90] Ching W Y, Mo S-D, Ouyang L, Rulis P, Tanaka I and Yoshiya M 2002 *J. Am. Ceram. Soc.* **85** 75–80

[91] Dong J, Deslippe J, Sankey O F, Soignard E and McMilliam P F 2003 *Phys. Rev.* B **67** 94104

[92] Soignard E and McMillam P F 2004 *Chem. Mater.* **16** 3533–42

[93] Soignard E, McMillam P F and Leinenweber K 2004 *Chem. Mater.* **16** 5344–9

[94] Soignard E, Machon D, McMillam P F, Dong J, Xu B and Leinenweber K 2005 *Chem. Mater.* **17** 5465–72

[95] Kresse G and Hafner J 1993 *Phys. Rev.* B **47** 558–61

[96] Kresse G and Furthmuller J 1996 *Comput. Mater. Sci.* **6** 15–50
Kresse G and Fur thmuller J 1996 *Phys. Rev.* B **54** 11169–86

[97] Charleir J-C, Blase X and Roche S 2007 *Rev. Mod. Phys.* **79** 677

[98] Lambin P 2003 *C.R. Phys.* **4** 1009

[99] Iannuzzi M 2008 *J. Chem. Phys.* **128** 204506 XANES of ice and water

[100] Wernet P, Nordlund D, Bergmann U, Cavalleri M, Odelius M, Ogasawara H, Naslund L A, Hursh T K, Ojamae L, Glatzel P, Pettersosn L G M and Nilsson L 2004 *Science* **304** 5763

[101] Soler J M, Artacho E, Gale J D, Garcia A, Junquera J, Ordejon P and Portal D S 2002 *J. Phys.: Condens. Matter* **14** 2745

[102] Bukowski R, Szalewicz K, Groenenboom G C and van der Avoird A 2007 *Science* **315** 1249

[103] Myneni S C B 2002 *Science* **295** 1039

[104] Longa S D, Arcovito A, Girasole M, Hazemann J L and Benfatto M 2001 *Phys. Rev. Lett.* **87** 155501

[105] Harris H H, Pickering I J and George G N 2003 *Science* **301** 1203

[106] Ouyang L, Randaccio L, Rulis P, Kurmaev E Z, Moewes A and Ching W Y 2003 *J. Mol. Struct. (Theo. Chem.)* **622** 221–7

[107] Kurmaev E Z, Moewes A, Ouyang L, Randaccio L, Rulis P, Ching W Y, Bach M and Neumann M 2003 *Europhys. Lett.* **62** 582–7

[108] Ouyang L, Rulis P, Ching W Y, Nardin G and Randaccio L 2004 *Inorg. Chem.* **43** 1235–41

[109] Ouyang L, Rulis P, Ching W Y, Slouf M, Nardin G and Randaccio L 2005 *Spectrochim. Acta* A **61** 1647–52

[110] Champloy F, Gruber K, Logl G and Kratky C 2000 *J. Synchrtron Radiat.* **7** 267–73

[111] Resta R 2008 *Nature* **453** 735

[112] Rabiger H, Lany S and Zunger A 2008 *Nature* **453** 763–6

[113] de Groot F 2001 *Chem. Rev.* **101** 1779

[114] Ogasawara K, Iwata T, Koyama Y, Ishii T, Tanaka I and Adachi H 2001 *Phys. Rev.* B **64** 115413

[115] Saldin D K and Ueda Y 1992 *Phys. Rev.* B **46** 5100–9

[116] Auerhammer J M and Rez P 1989 *Phys. Rev.* B **40** 2024–30

[117] Scahattschneider P, Rubino S, Hebert C, Rusz J, Kunes J, Novak P, Carlino E, Fabrizioli M, Pannaccione G and Rossi G 2006 *Nature* **441** 486

[118] Kotani A and Shin S 2001 *Rev. Mod. Phys.* **73** 203

[119] Nordgren E J and Kurmaev E Z (ed) 2000 *Soft X-Ray Emission Spectroscopy* (Amsterdam: Elsevier) (Special Issue in *J. Elect. Spectros. Rel. Phenomena*)

[120] Rulis P, Pennycook S J, Rupini A and Ching W Y 2008 in preparation